

Guided Waves in Embedded Concrete Piles

Richard J. Finno, M.ASCE,¹ and Hsiao-chou Chao, A.M.ASCE²

Abstract: Results of a three dimensional (3D) guided wave evaluation of the stress waves generated by the impulse response method show that the conventional interpretation technique based on 1D wave propagation theory is essentially a special application of the first branch of longitudinal wave modes with frequency components up to several thousand hertz. To extend the frequency range and incorporate special wave characteristics of higher modes so that the integrity of an embedded pile can be evaluated in a more thorough manner, a frequency-controlled method capable of exciting waveforms with higher and selective frequency components is introduced to nondestructively evaluate prototype concrete piles. Experimental results on a prototype pile are analyzed by processing the responding signals in the joint time–frequency domain, then comparing the processed waveforms with the theoretically computed results. These results show that the mode attributes of the experimentally excited waves are consistent with the results of theoretical evaluations. Based on this finding, this guided wave approach can be applied to evaluate the integrity of a drill shaft with appropriately determined parameters of the soil–pile system.

DOI: XXXX

CE Database subject headings: Nondestructive tests; Concrete piles; Drilled shafts; Wave propagation; Energy dissipation.

Introduction

Nondestructive evaluation techniques have been used for decades to provide quality assurance for drilled shafts and driven concrete piles. Surface reflection techniques such as sonic-echo and impulse response methods have been used extensively to inspect the continuity and length of newly installed drilled shafts. These methods can be conducted inexpensively and quickly. The sonic echo method evaluates the integrity of a drilled shaft by interpreting the time domain wave trace of the measured surface vibrations triggered by a hammer impact. The impulse response method considers both the impact force and surface vibration variations with time. The integrity of a drilled shaft can be evaluated by comparing the experimentally derived frequency response of the drilled shaft and the numerically simulated frequency response based on construction data, design details, and soil parameters. Anomalies in a drilled shaft can be detected by identifying discrepancies in the results between the experimental data and numerical results. The location and type of an anomaly can be identified in certain instances by finding the best matched input parameters using a numerical simulation program (e.g., Davis, unpublished computer program, STS Consultants, Deerfield, Ill 1994; Finno and Gassman 1998).

In spite of the success of the conventional surface reflection technique, the practical application of these nondestructive evalu-

ation methods are subject to certain limitations as a result of the inherent properties of the stress waves generated by a typical hammer impact. The wavelength of the propagating stress wave is large—at least larger than the diameter of the pile. The frequencies of the hammer-generated stress waves are low—typically less than 1,000 Hz. The relatively large wavelengths are not affected by small anomalies and thus cannot be used to identify such anomalies. One way to extend the applicability of the conventional surface reflection techniques, is to increase the input frequency such that waves with smaller wavelength are induced in the shaft. Smaller anomalies will affect the propagation of waves with smaller wavelengths and hence can be identified.

A theoretical guided wave approach for evaluating the integrity of a drilled shaft was presented by Hanifah (1999) and Finno et al. (2001). This three-dimensional numerical approach was developed by treating a drilled shaft as an embedded waveguide. A waveguide is an extended body with a cross section of finite dimensions within which stress waves propagate in the extended direction despite the occurrence of the incident and reflected waves at the boundaries (Achenbach 1973). Although local disturbances decay rapidly in three-dimensional space in wave propagation problems, typical waveguides, such as long hollow tubes, circular bars, and plates, permit wave propagation in one or two dimensions. Based on this concept, an embedded pile can be treated as a waveguide that allows a transient pulse introduced through the pile head. The continuing interaction of the excited waves with the boundaries produces the frequency-dependent guided waves.

The objective of this paper is to provide experimental verification of the guided wave theory and to evaluate the applicability of the theoretical guided wave approach on embedded prototype cylindrical piles. Theoretical solutions in terms of dispersion curves were derived by substituting the experimentally determined soil and concrete parameters into the longitudinal mode frequency equation. The theoretical results at higher frequencies are verified herein by results of specially designed tests wherein waves with a relatively narrow frequency range are induced in a

¹Professor, Dept. of Civil Engineering, Northwestern Univ., 2145 Sheridan Rd., Evanston, IL 60208.

²Post-Doctoral Research Associate, Dept. of Civil Engineering, Northwestern Univ., 2145 Sheridan Rd., Evanston, IL 60208.

Note. Discussion open until June 1, 2005. Separate discussions must be submitted for individual papers. To extend the closing date by one month, a written request must be filed with the ASCE Managing Editor. The manuscript for this paper was submitted for review and possible publication on August 11, 2003; approved on April 19, 2004. This paper is part of the *Journal of Geotechnical and Geoenvironmental Engineering*, Vol. 131, No. 1, January 1, 2005. ©ASCE, ISSN 1090-0241/2005/1-1-XXXX/\$25.00.

pile. In this frequency-controlled wave excitation method, the acquired signals were analyzed by various signal processing technologies including digital filtering, fast Fourier transform (FFT), and short time Fourier transform (STFT).

Background

Guided waves in a pile are combinations of longitudinal and shear waves that in turn continually interact with the boundaries to produce a composite wave (Pavlovic et al. 1998). Based on work by Zemanek (1971) and Thurston (1978), Hanifah (1999) presented the general frequency equation for a steady-state wave propagating along infinitely long embedded piles. The numerical solution elucidates the propagation modes that represent various motions that can be excited in a pile. The general solution is simplified when examining the longitudinal modes of vibration, and the results can be expressed in terms of group velocity and attenuation dispersion relations, and the modal shape.

Each solution of the frequency equation is termed a “mode.” Each mode can be characterized by the group velocity, phase velocity, and the attenuation coefficient. The vibrations across the pile excited by the energy carried by a particular wave mode are expressed as the displacement distribution profile. For a given wave mode, the displacement distribution can be computed. Theoretically, one can select points at the pile surface having the maximum vibration amplitude to measure the vibration signals because the acquired signals should have the optimal signal to noise ratio (SNR), and hence be able to reveal the pile response.

The axisymmetrical mode frequency equation can be numerically solved in terms of the density ratio ρ_p/ρ_s , shear modulus ratio μ_p/μ_s , and Poisson's ratio (ν) of the soil and pile. The subscripts p and s refer to pile and soil, respectively. The solutions can be expressed as dispersion relations in terms of nondimensional frequency Ω versus the nondimensional wave number Ξ defined as

$$\Omega = \frac{2\pi fa}{c_T} \quad (1)$$

$$\Xi = \xi a \quad (2)$$

where f =dimensional frequency; a =pile radius; c_T =shear wave velocity in the pile material; and ξ =complex wave number.

The axisymmetrical mode waves are represented by the notation $L(0,m)$ where L stands for the longitudinal mode, 0 represents the order of the Hankel function in the frequency equation, and m is the m th branch of the axisymmetric mode solutions. The imaginary part of the solution can be developed to yield the geometric attenuation of the energy and the real part of the solution can be used to compute the phase and group velocities of the propagating waves.

Dispersion curves for the first three branches of the axisymmetric modes are shown in Fig. 1 for three values of shear modulus ratio. Fig. 1(b) illustrates the real parts of the solutions are independent of the shear modulus ratio, density ratio, and Poisson's ratio of surrounding soils. Hence the propagating velocity is only affected by the Poisson's ratio of the concrete (Hanifah 1999). The imaginary part of dispersion curves varies with each of the input parameters. For a given pile, the larger the shear modulus ratio, and hence the lower the shear wave velocity of the soil, the smaller the imaginary part of wave number at any give frequency, and hence the smaller the geometric attenuation.

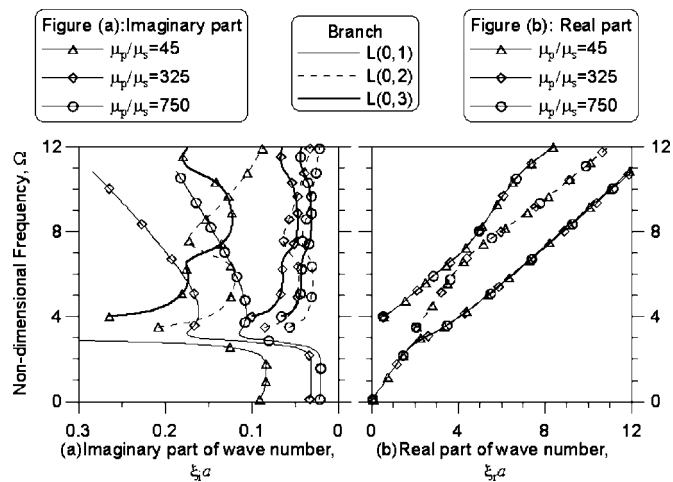


Fig. 1. Effects of shear modulus ratio on solutions of longitudinal mode frequency equation

The results of numerical evaluations allows one to define guidelines for applying the guided wave theory to evaluate the integrity of piles. Generally, the frequency range that is preferable for guided wave tests should satisfy the following criteria:

1. Within the selected frequency range, the modes along the same longitudinal branch have an approximately constant group velocity.
2. The attenuation coefficients of wave modes in a selected frequency range have to be small enough so that the waves expected to be excited are able to reflect back and be identified.
3. For the acquired waveforms to have better signal to noise ratio and an apparent mode attribute that can be identified, the transducers should be mounted at the points having the maximum vibration amplitude excited by the expected wave modes.
4. If more than one mode is excited at a frequency of interest, the difference between the mode characteristics of different branch of modes need to be distinguishable so that the mode attributes of each waveform can be identified.

A method to control the frequency content of the excited waveform has been presented by Chao and Finno (private communication 2003). This approach was essentially modified from the method developed by Popovics et al. (1999) in which the frequency-controlled waves on concrete structures were excited by modal shakers. The input waveform is composed of a finite number of sine waves or square waves. The central frequency f_c of the input waveform is controlled by the cycle frequency of the waveform composed of the input waves, and the bandwidth of the input waveform is controlled by the number of the cycled waveform. The control of a waveform composed of narrow band frequency components can be achieved by using a large number of cycles of waves for the input waveform. However, the total duration of the input waveform is limited by the length of the piles being tested in practice. When a waveguide does not provide enough travel length, the reflections will be masked by the surface vibrations induced by input waveform, greatly complicating the data analysis.

The shear wave velocity c_T can be computed from the measured bar wave velocity c_B

$$c_T = \frac{c_B}{\sqrt{2 \cdot (1 + \nu)}} \quad (3)$$

This approach, however, requires accurate determination of ν of the pile. Chao and Finno (private communication 2003) presented an approach for determining the shear wave velocity of a concrete cylinder by experimentally identifying the universal mode frequency. Theoretical evaluation shows that for each longitudinal branch, there exists a wave mode with group and phase velocities and geometric attenuation independent of Poisson's ratio. For the $L(0,1)$ branch, the nondimensional universal frequency was numerically determined as 2.60. By identifying the frequency f_{UM} corresponding to the nondimensional universal frequency of 2.60 from experimental results, the shear wave velocity can be determined by

$$c_T = \frac{2\pi \cdot f_{UM} a}{2.60} \quad (4)$$

where a =radius of the concrete pile. Thus, the dependence on ν is removed from the evaluation and, hence, uncertainty in the measured shear wave velocity is reduced.

The travel time Δt of a wave propagating along a pile can be found directly from the measured waveforms in the time domain. The acquired waveforms essentially are a superposition of waves with different frequency components. If a wave packet is composed of waves with approximately the same group velocity, the group wave velocity c_g can be calculated in the manner

$$c_g = \frac{2L}{\Delta t} \quad (5)$$

where $2L$ =propagation distance for an anomaly-free pile with length L . The calculated wave velocity represents the weighted average of the group velocity of all the wave modes carried by the observed wave packet of interest in the excited frequency band.

Fundamental wave propagation theory indicates that resonance occurs when the integral number of half wavelength $\lambda/2$ equals to the pile length L

$$L = \frac{n\lambda}{2} \quad (6)$$

where n =harmonic number. By measuring the resonant frequency, the phase velocity can be computed subsequently. When the pile length is known, the phase velocity c_p corresponding to the resonant frequency can be computed by

$$c_p = f_n \cdot \lambda \quad (7)$$

where f_n represents the resonant frequency.

The conversions between the theoretical nondimensional and experimental dimensional solutions of frequency and group velocity are made by substituting the shear wave velocity c_T into the following equations:

$$f = \frac{c_T \cdot \Omega}{2\pi a} \quad (8)$$

$$c_g = C_g c_T \quad (9)$$

where c_g represents the dimensional group velocity with the same units as c_T , and C_g represents the numerically derived nondimensional group velocity. The dimensional solution of attenuation ξ_i can be derived from dividing the nondimensional geometrical attenuation coefficient Ξ by pile radius a using Eq. (2).

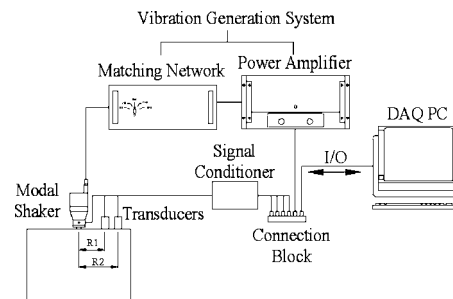


Fig. 2. System setup for frequency-controlled tests

Prototype Piles and Soil Conditions

The applicability of the theoretical nondestructive guided wave approach was evaluated with two prototype piles: B10-222 and B12-240. The "10" and "12" after B refer to the pile diameter in inches and the "222" and "240" refer to the length of the pile in centimeters. These concrete piles were carefully cast in laboratory and installed in the National Geotechnical Experimental Site at Northwestern University (NU-NGES). The concrete was cast with a water-cement ratio of 0.5, a fine aggregate-cement ratio of 2.0, and a coarse aggregate-cement ratio of 2.3. The mean dynamic shear moduli and the mean density of this concrete were 14.3 GPa and 2,325 kg/m³, respectively, based on the experimental approach proposed by Subramaniam et al. (2001).

Results of cross-hole seismic tests reported by Gassman (1997) indicated the shear wave velocity of the upper sand fill at the NU-NGES varies from 110 to 115 m/s and the density ρ_s ranges from 1,500 to 1,550 kg/m³. The corresponding shear moduli computed from elastic theory vary between 18.2 and 20.5 MPa. The shear wave velocities were found to be 2,920 m/s for B12-240 and 2830 m/s for B10-222 following the approach presented in Chao and Finno (private communication).

Concrete and soil parameters identified experimentally were subsequently combined to form the input parameters for the longitudinal mode frequency equation. The solutions of the longitudinal mode frequency equation in terms of dispersion relations were derived based on a shear modulus ratio of 740, a density ratio of 1.5, a Poisson's ratio of soil of 0.3, and Poisson's ratios of concrete from 0.14 to 0.28. The selected solutions are used as the baseline for data analysis.

Experimental Apparatus and Procedures

The input vibrations can be induced herein by either hammer impact or controlled modal shaker vibrations. The method to generate stress waves by hammer impact has been reported in many references (e.g., Finno and Gassman 1998). Popovics et al. (1999) presented an approach to excite frequency-controlled waves in concrete structures using modal shakers. Fig. 2 shows the experimental system for frequency-controlled tests that is composed of a vibration generation system, a vibration measurement assembly, and a PC-based control system. The vibration sources include both modal hammers and a modal shaker. A modal hammer can be used to generate stress waves with a broad band of frequency components up to several thousand Hertz. Because longitudinal waves are dispersive at higher frequencies, for higher frequency applications, the frequency content of the waves is controlled by a piezoelectrical modal shaker. The excited vibrations are measured by charge-mode accelerometers that have wide and flat frequency

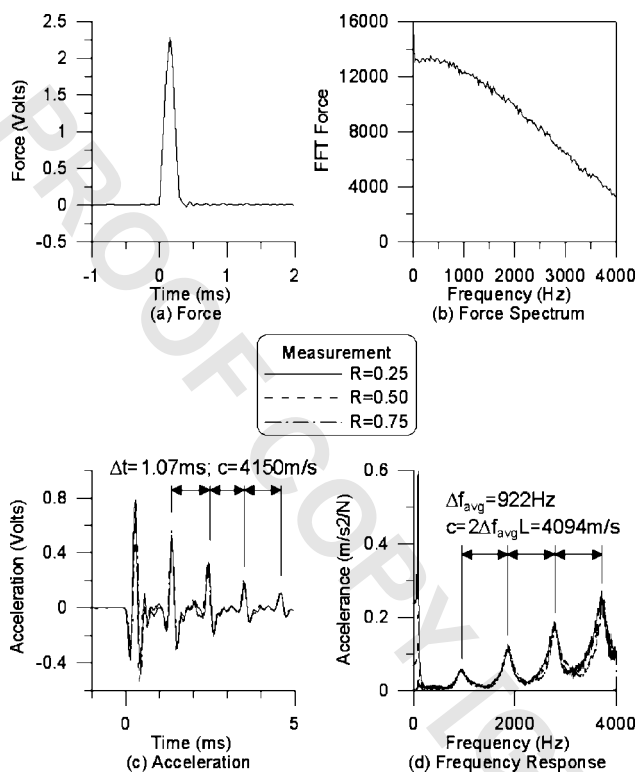


Fig. 3. Results of impulse response test for B10-222

responses mounted vertically on top end of the prototype piles. The acquired vibration signals are sent back to the PC-controlled system, consisting of a portable personal computer with a PCI multifunction data acquisition board and a virtual control program.

The PC-based control system is able to perform the functions of both pulse generator and digital oscilloscope. The vibration shaker is controlled by waveform signals modulated by a virtual pulse generator and power amplifier. The control parameters for this virtual pulse generator include point update rate, number of points in one period, total number of updates, generation counts, and voltage limits where point update rate defines the time interval between two generated vibration spikes. The number of points in one period gives the composition of the waveform. The total number of updates and generation counts determines the length of the pulse or the number of wave cycles included in the pulse. Data averaging and spectral analyses are programmed as part of the virtual oscilloscope program so that the preliminary evaluation of the test results can be done in real time. A more detailed description of this PC-controlled data acquisition system is presented by Chao and Finno (private communication 2003).

Results and Analysis

Impulse Response Tests

Fig. 3 shows the results of an impulse response test on embedded pile B10-222 in terms of force versus time, acceleration versus time, FFT force spectrum, and the accelerance response. The propagation velocity presented in Fig. 3(c) was determined from the the measured acceleration waveform by dividing the propagation distance $2L$ with the averaged time intervals between waveform peaks. This propagation velocity can also be determined

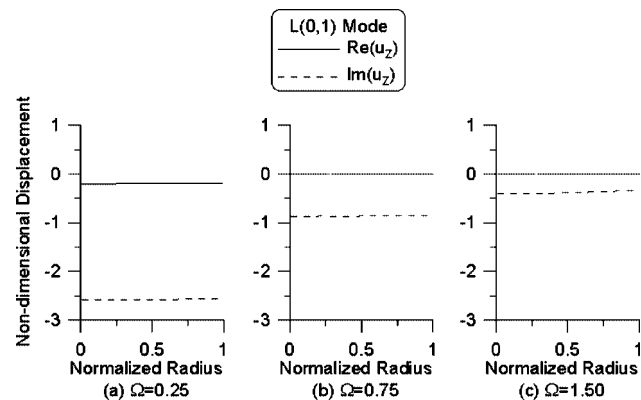


Fig. 4. Computed displacement profiles of $L(0,1)$ modes at: (a) $\Omega=0.25$, (b) $\Omega=1$, and (c) $\Omega=1.5$

from the frequency response of the pile in terms of acceleration by multiplying the averaged resonant interval Δf by the known propagation distance $2L$, as shown in Fig. 3(d).

The excited vibrations were measured simultaneously at three locations on the pile, expressed in terms of the nondimensional radius R

$$R = \frac{r}{a} \quad (10)$$

where a =radius of the pile and r =distance to the center of the pile. Results in Figs. 3(c and d) show that the magnitudes of the reflection signals measured at $R=0.25$, 0.5 , and 0.75 are practically the same.

Fig. 4 shows the computed displacements normalized by the energy propagating along the pile based on guided wave theory, as described by Hanifah (1999) and Finno et al. (2001). The solutions marked real and imaginary in Fig. 4 represent the displacements at 90° phase angles; hence the normalized displacement magnitudes are expected to vary between these two limits—the greater the separation, the greater the observed displacement. As can be seen, the vibration amplitude of each of the three modes is uniformly distributed across the radius of the pile, implying that a plane wave propagates along the pile. Thus the observed results in Fig. 3 are consistent with those computed based on guided wave theory.

Fig. 5 shows the phase velocities computed from Eq. (7) at the resonant frequencies for the two piles superimposed onto the numerically derived $L(0,1)$ branch dispersion curves for pile Poisson's ratios varying between 0.14 to 0.28. A shear wave velocity was computed from Eq. (3) for each Poisson's ratio based on the assumption that the bar wave velocity is equal to the propagation velocity measured from the time-domain waveform, and is used for the conversion between dimensional and nondimensional solutions. By comparing the measured phase velocities and the converted theoretical dispersion curves, a "best-fit" numerical solution can be identified. The dispersion curves are characterized by the Poisson's ratio of 0.25, and 0.28 for piles B10-222 and B12-240, respectively. As expected at low frequencies for one dimensional wave propagation, these phase velocities are practically equal to the group velocities computed from the time domain results, although the trend of decreasing phase velocity with frequency is clearly seen.

For embedded piles, the distance that an axisymmetrical wave is able to travel is controlled by both the geometrical and material attenuation. Theoretically, the radially lost energy can be quanti-

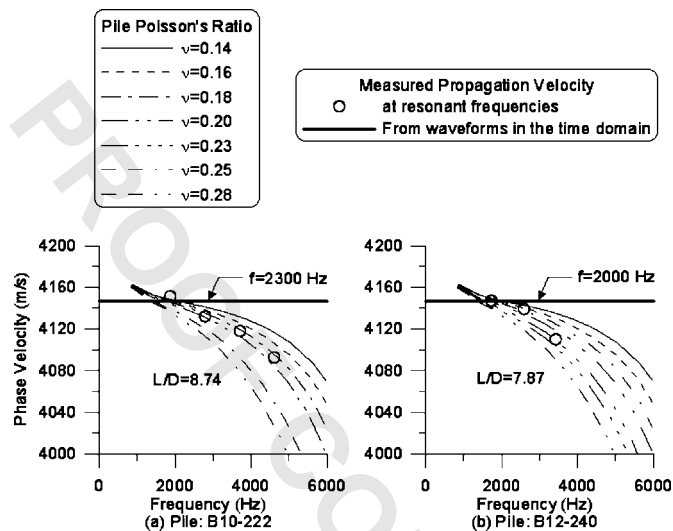


Fig. 5. Phase velocities measured based on time-domain waveform and resonant peaks superimposed by numerically derived phase velocity dispersion curves with Poisson's ratio from 0.14 to 0.28: (a) pile B10-222 and (b) pile B12-240

tatively computed from the numerically derived attenuation coefficient. In practice, however, the measurable attenuation is a superimposed effect of the energy loss caused by the radially dissipated waves, material damping, and the waves that flow outward through the tip of the pile. Material damping is a result of the scattering and absorption of waves at the interfaces between the aggregate and cement. The energy loss at the tip of the pile arises because part of the wave energy is transmitted into the soil below the tip of the pile and part of it is reflected back.

The total attenuation of the propagating waves along a concrete pile can be calculated by substituting the time and amplitude between two waveform peaks into the equation

$$\ln(A) = \alpha t + \beta \tag{11}$$

where A =measured magnitude of waveform peak; and α, β =coefficients derived from the linear regression. The attenuation calculated can be compared to that based on the imaginary part of wave number of the numerically derived dispersion curve from

$$\ln\left(\frac{A_1}{A_2}\right) = \alpha(t_1 - t_2) \tag{12}$$

$$= \alpha \Delta t \tag{13}$$

$$= \alpha \frac{\Delta L}{c} \text{ (neper)} \tag{14}$$

$$\frac{\ln\left(\frac{A_1}{A_2}\right)}{\Delta L} = \frac{\alpha}{c} \text{ (neper/length)} \tag{15}$$

$$\frac{\alpha}{c} = \xi_i \text{ (neper/length)} \tag{16}$$

where ΔL represents the propagation distance over the time interval Δt between waveform peaks.

For attenuation expressed in decibels per unit length, Eqs. (15) and (16) can be rewritten as

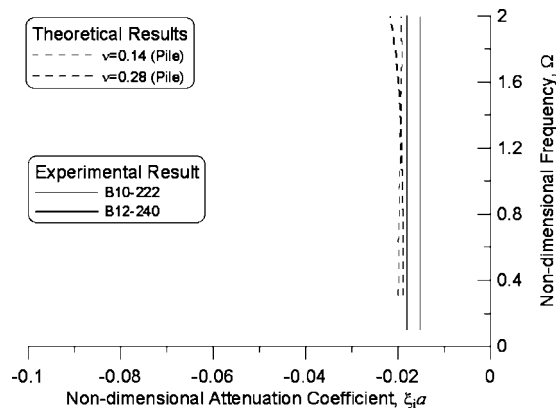


Fig. 6. Comparison between experimental and computed attenuation coefficients

$$\frac{20 \log\left(\frac{A_1}{A_2}\right)}{\Delta L} = 8.686 \frac{\alpha}{c} \text{ (dB/length)} \tag{17}$$

$$= 8.686 \xi_i \text{ (dB/length)} \tag{18}$$

The attenuation calculated by Eq. (15) can be further normalized by Eq. (2) with the pile radius, a .

Fig. 6 shows a comparison between the numerically developed attenuation dispersion curves with $\nu=0.14$ and 0.28 within the frequency range from $\Omega=0-1.6$ and the attenuation coefficients experimentally computed based on the assumption that all the wave components have the same attenuation coefficient. This result shows that even though the directly measured attenuation is theoretically a superimposed effect of the material damping and geometrical attenuation, in practice, the total attenuation can be approximated from the numerically derived attenuation dispersion curve at least at these frequencies.

The agreements between the results of the impulse response tests and the numerical analysis in group velocity, phase velocity, and attenuation, show that the attributes of the waves generated by hammer impact are primarily the $L(0,1)$ mode. These results also suggest that for impulse response tests, the location of the measurement across the pile does not have significant influence on experimental results which is consistent with the assumption of plane wave propagating in conventional tests.

Frequency-Controlled Tests

Results of the impulse response test show that the conventional surface reflection technique is essentially an application of the particular characteristics of the first branch of the longitudinal mode solutions in the lower frequency range. The limits of the frequency range where the assumption of plane waves and, hence, nondispersive wave propagation, is valid have been discussed by Finno et al. (2001). To extend the useful frequency range, one must consider the effects of dispersion on the wave propagation. Ideally, when one induces high frequency waves into a pile, the energy should be composed of waves with relatively constant propagation velocity and low attenuation. The high frequency waves need to be excited by a frequency-controlled method. Because the mode shape will not be uniform at higher frequencies, the surface vibrations need to be measured at locations with optimal SNR across the pile, hence the mode shape must be incorporated into the data analysis.

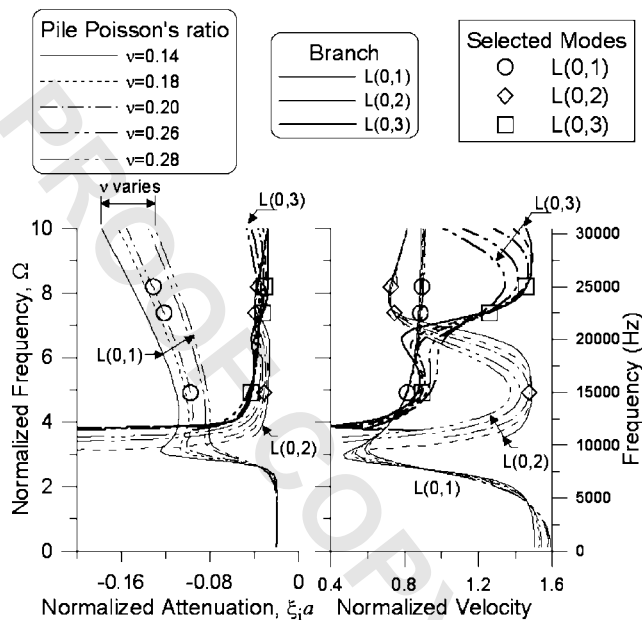


Fig. 7. Numerically derived group velocity and attenuation dispersion curves and selected modes at $f=15$, 22.5, and 25 kHz for embedded pile B12-240

Experimental results of pile B12-240 are used to demonstrate the frequency-controlled method. The excited vibrations were measured simultaneously by accelerometers at normalized radii R of 0.25 and 0.75 to evaluate the relationship between the mode attributes of the acquired signals and the numerically computed displacement distribution profiles. The recorded signals were averaged from 100 repetitive wave excitations and signal acquisitions. The averaged signals were then pass through a Butterworth filter with lowpass cutoff frequency of 30 kHz to eliminate unwanted noise. The processed signals were subsequently transformed to the joint time–frequency domain by the STFT algorithm (e.g., Vaidyanathan 1993) so that the frequency contents of the reflection waves can be evaluated as a function of time. To compare the experimental results directly with the numerically derived group velocity dispersion curves and to identify the mode attribute of the reflection waves the joint time–frequency spectrograms are thereafter normalized to the joint velocity–frequency domain by the radius a , length L , and the shear wave velocity c_T of the pile.

Fig. 7 shows the numerically derived group velocity and attenuation dispersion curves based on the applicable density ratio

$\rho_p/\rho_s=1.5$, shear modulus ratio $\mu_p/\mu_s=740$, and Poisson's ratio of the soil $\nu_s=0.3$, and Poisson's ratios of the concrete from $\nu_p=0.14$ to 0.28. Both nondimensional and dimensional frequency coordinates are shown on the figure; the latter frequency is converted from the nondimensional solution by the pile radius $a=0.15$ m and the shear wave velocity $c_T=2,920$ m/s, using Eq. (8). The wave modes selected for evaluating the pile have frequencies of $f=15,000$, 25,000, and 22,500 Hz. At 15,000 and 25,000 Hz, the group velocities have an approximately constant velocity. The group velocities for the $L(0,2)$ and $L(0,3)$ modes at these frequencies are different enough so that the arrival of the waveforms can be distinguished. Another frequency of $f_c=22,500$ Hz was selected to evaluate whether or not the waveforms can be analyzed if a selected wave mode is within a frequency range where the group velocity changes significantly. Table 1 lists the nondimensional and dimensional solutions of the attenuations and group velocities of these selected modes. The computed attenuation coefficients in Table 1 imply the reflection waves will be primarily composed of $L(0,2)$ and/or $L(0,3)$ waves, because the $L(0,1)$ mode waves will attenuate at rates 3–4 times more than the higher modes. For example, at a frequency of 22,500 Hz, if one assumes that the amplitudes of the excited $L(0,1)$, $L(0,2)$, and $L(0,3)$ modes are equal to one, and the material attenuation and the attenuation from the bottom of the pile can be neglected, the amplitudes of the reflection waves will be 0.02, 0.29, and 0.36, respectively, based on Eq. (18). It is not difficult to envision that if the three selected wave modes are all excited at this frequency, then the observed waves should be the $L(0,2)$ and $L(0,3)$ modes, because the $L(0,1)$ mode waves would be small compared to the other two modes.

Figs. 8–10 show the results of the frequency-controlled tests at $f_c=15$, 25, and 22.5 kHz, respectively. The force and acceleration signals in parts (a), (b), and (c) are the waveforms averaged from 100 repetitive waveform excitations and acquisitions and processed by the Butterworth filter with lowpass frequency of 30 kHz. The time domain waveform traces were then transformed to the joint time–frequency domain by the STFT algorithm. The results of STFT transformation are presented as the spectrograms shown in parts (d) and (e). One of the advantages of using STFT is that the frequency contents of the observed waves can be evaluated on the time basis. If the mode attribute of an observed wave is different from the input waves, mode conversion can be perceived directly from the spectrogram. Results of observations indicate that no mode conversion occurs in these frequency-controlled tests, as observed in the plots in Figs. 8–10, where the maximum values of the reflections in (b) and (d) and in (c) and (e) occur at the same time. The observed waves are marked A, B, C,

Table 1. Attenuation Coefficients and Group Velocities of Selected Modes

Frequency Ω	Attenuation coefficient			Group velocity		
	$L(0,1)$	$L(0,2)$	$L(0,3)$	$L(0,1)$	$L(0,2)$	$L(0,3)$
	$\xi_i a$ (neper)			Nondimensional C_g		
4.19	-0.10	-0.03	-0.04	0.81	1.47	0.89
7.38	-0.12	-0.04	-0.03	0.89	0.75	1.26
8.2	-0.13	-0.04	-0.03	0.89	0.73	1.46
f (Hz)	ξ_i (dB)			c_g (m/s)		
15,000	-26.72	-8.47	-11.67	2,380	4,310	2,610
22,500	-33.20	-10.65	-8.90	2,590	2,180	3,680
25,000	-35.90	-10.06	-8.41	2,610	2,120	4,260

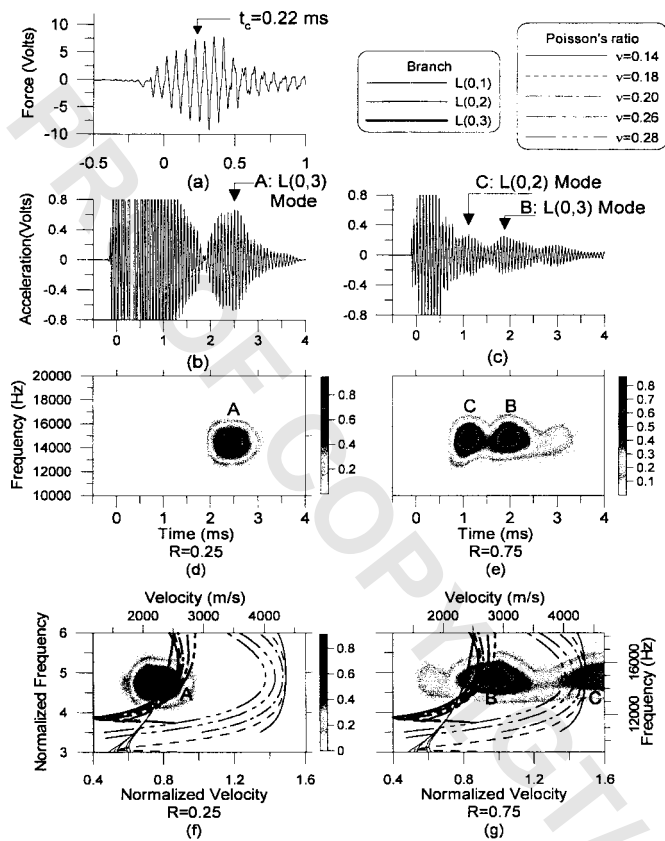


Fig. 8. Results of frequency-controlled test at $f_c=15,000$ Hz ($\Omega=4.91$) for pile B12-240

and D in the time-domain waveforms and spectrograms. The magnitudes of the observations in parts (d)–(g) are shown by the shading in each figure—the nearer the center of the shading, the larger the magnitude of the response.

To directly compare the numerically derived and observed group velocity dispersion curves and to identify the mode attribute of the reflection waves, the time and frequency coordinates of the spectrograms t_i and f_j are converted into the nondimensional velocity and frequency coordinates C_i and Ω_j in parts (f) and (g) in Figs. 8–10 by the propagating distance D , the radius of the pile a , the shear wave velocity c_T , and the reference time t_c , for computing the arrival of reflection waves using Eqs. (1) and (9). The propagating distance D for the first wave reflection is twice the length of the pile $2L$. The reference time t_c is the time coordinate of the center of the input waveform. Results of the identification are summarized in Table 2 which shows that for $f_c=15,000$ Hz (Fig. 8), the mode attributes of the primary reflection waves acquired at $R=0.25$ are the $L(0,3)$ modes while at $R=0.75$ are the $L(0,2)$ and $L(0,3)$ modes. For $f_c=25,000$ Hz (Fig. 9) and $22,500$ Hz (Fig. 10), both the $L(0,2)$ and $L(0,3)$ modes are composed of the primary reflections acquired at $R=0.25$ and 0.75 .

Evaluation on the numerically derived attenuation dispersion curves (see Fig. 1) shows that the $L(0,1)$ mode has a much larger attenuation than the higher modes, and hence one would not expect to observe this mode at these high frequencies. This is consistent with the experimental results shown in Figs. 8–10.

Fig. 11 shows the displacements profiles of the $L(0,1)$, $L(0,2)$, and $L(0,3)$ mode of waves at the selected frequencies. In this figure, the displacements are normalized by the energy propagating along the pile, as described by Hanifah (1999) and Finno et al.

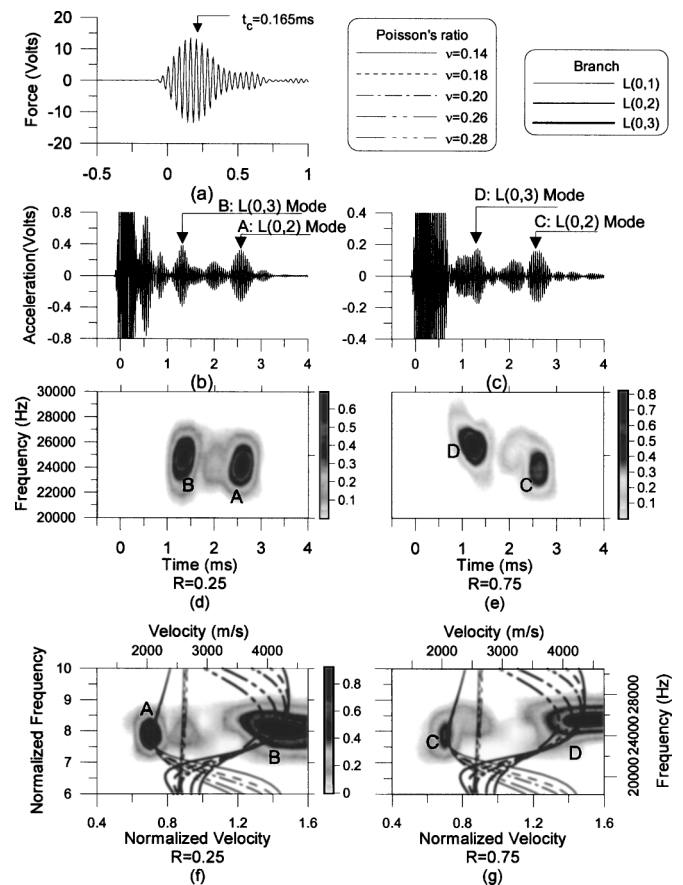


Fig. 9. Results of frequency-controlled test at $f_c=25,000$ Hz ($\Omega=8.2$) for pile B12-240

(2001). The solutions marked real and imaginary represent the displacements at 90° phase angles; hence the normalized displacement magnitudes are expected to vary between these two limits—the greater the separation, the greater the observed vibration amplitude. As can be seen in Fig. 11(a), the amplitudes of the $L(0,1)$ and $L(0,2)$ modes at $R=0.25$ are small compared to that of the $L(0,3)$ mode at $f_c=15,000$ Hz. At $R=0.75$, the vibration amplitudes are similar for the $L(0,2)$ and $L(0,3)$ modes. Therefore, at $R=0.25$, only the $L(0,3)$ mode can be identified and at $R=0.75$, both the $L(0,2)$ and $L(0,3)$ modes can be found. Based on the same consideration with Figs. 11(b) and (c), it is not difficult to envision that at $f_c=22,500$ and $25,000$ Hz, the $L(0,2)$ and $L(0,3)$ modes are both identified at $R=0.25$ and 0.75 .

Ideally, the propagating waves excited by the frequency-controlled method are composed of waves with frequency components within a narrow frequency band. Within this frequency band, if all the wave components propagate at a constant velocity, the arrival of the reflection waves, which are essentially a superimposed waveform of all the excited wave components, can be more easily interpreted. The frequencies of $f_c=15,000$ and $25,000$ Hz were selected because the equivalent nondimensional frequencies $\Omega=4.91$ and 8.20 , respectively, are within the frequency ranges where the group velocities do not vary significantly with small changes of frequencies. However, joint-time frequency analyses (JTFA), such as the STFT shown in (f) and (g) of Figs. 8–10, are alternative means of analyzing guided waves that can be used as a check on the interpreted result. As shown in Fig. 7, the theoretically derived group velocities vary significantly with small change of frequency near $f=22,500$ Hz ($\Omega=7.38$).

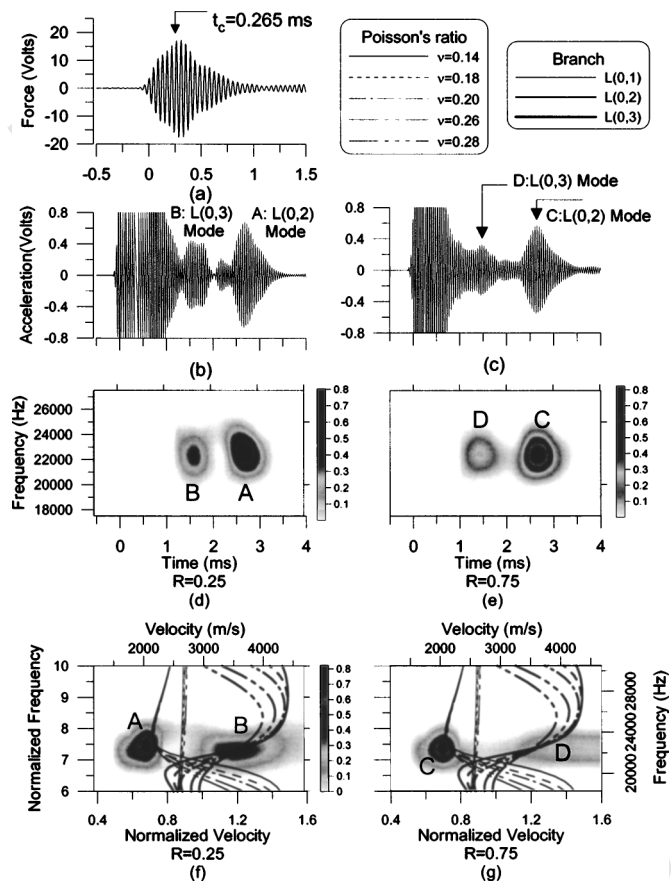


Fig. 10. Results of frequency-controlled test at $f_c=22,500$ Hz ($\Omega=7.38$) for pile B12-240

Nevertheless, the mode attributes of the reflection waves can still be identified from the normalized spectrograms transformed by STFT by the JTFA approach.

Results of the foregoing examples show that, for an embedded prototype pile without any designed defect, the mode attribute of an experimentally excited wave is found to be consistent with the result of numerical computation. Evaluation also shows that measurement points having a large enough SNR are located at points described by the numerical procedure. Because the experimental results match the theoretical results, the integrity of an embedded prototype pile can be evaluated based on the approach presented herein.

Fig. 12 shows the suggested procedures of nondestructive guided wave evaluation for embedded piles. This flow chart is developed based on the idea that the integrity of a pile can be evaluated by comparing the experimental results of the frequency-controlled test with the numerical results computed

Table 2. Summary of Mode Attributes of Reflecting Waves at Selected Locations

Frequency		Normalized radius, R	
f (Hz)	Ω	0.25	0.75
15,000	4.91	$L(0,3)$	$L(0,3), L(0,2)$
25,000	8.20	$L(0,3), L(0,2)$	$L(0,3), L(0,2)$
22,500	7.38	$L(0,3), L(0,2)$	$L(0,3), L(0,2)$

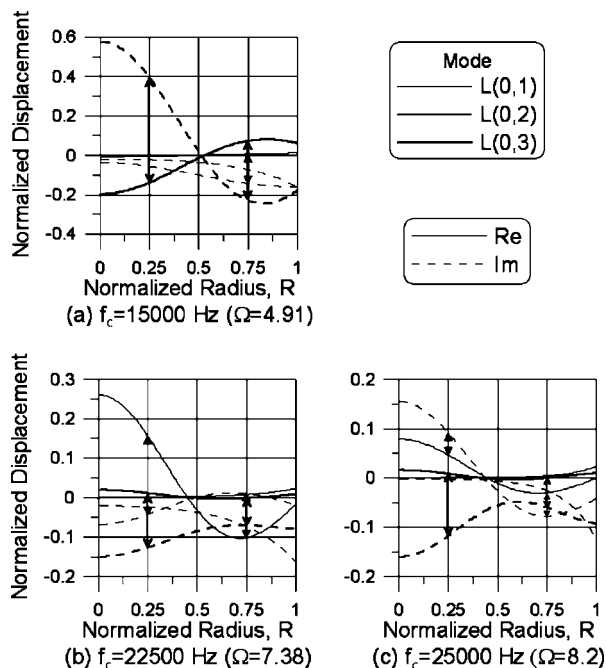


Fig. 11. Computed displacement profiles of $L(0,1)$, $L(0,2)$, and $L(0,3)$ modes at selected frequencies $f_c=15, 22.5,$ and 25 kHz

based on the data retrieved from construction records and results of site characterization. The integrity of the pile can be assured if the experimental and numerical results are consistent with each other. Otherwise, this procedure needs to be recursively performed by assuming a different location of the reflection source until the reflection source can be identified.

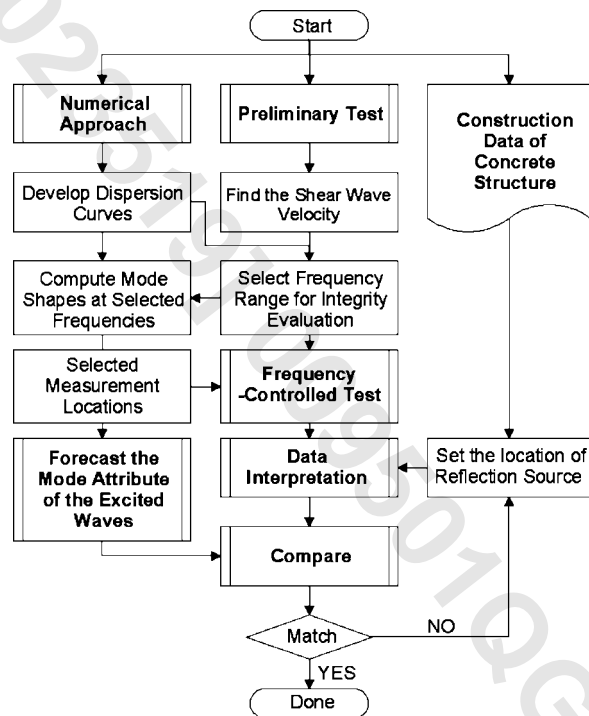


Fig. 12. Flow chart of nondestructive integrity evaluation for embedded piles using guided wave approach

Conclusions

Based on the numerical and experimental results presented herein, the following conclusions can be drawn relative to the frequency-controlled testing of concrete prototype piles:

1. The wave modes experimentally identified within a selected frequency range are consistent with the results of theoretical evaluation. This mode identification is conducted by transforming the acquired time-domain waveforms to the joint velocity-frequency domain by the STFT algorithm. The joint velocity-frequency spectrogram then is normalized so that the experimental results can be compared directly with the theoretically derived group velocity dispersion curves by superposition of the two results.
2. Observed responses at high frequencies are dependent on the location of the accelerometer. Results from guided wave theory can provide guidance as to where the transducers should be located.
3. Observed responses at high frequencies are dependent upon the geometric attenuation of the guided waves. The $L(0,1)$ mode waves have higher attenuation coefficients than higher modes [e.g., $L(0,2)$ and $L(0,3)$] when the nondispersion frequency exceeds about 2. Therefore one would not expect to see these modes at nondimensional frequencies greater than 2.

Acknowledgments

Support of this work was provided by a grant from the Infrastructure Technology Institute at Northwestern University. The continuing interest of its director, Mr. David Schultz, is greatly ap-

preciated. The writers also thank Professor John S. Popovics for his input throughout this work.

References

- Achenbach, J. (1973). *Wave propagation in elastic solids*, 1st Ed., North-Holland, Amsterdam, The Netherlands.
- Finno, R., and Gassman, S. (1998). "Impulse response evaluation of drilled shafts." *J. Geotech. Geoenviron. Eng.*, 124(10), 965–975.
- Finno, R., Popovics, J., Hanifah, A., Kath, W., Chao, H.-C., and Hu, Y.-H. (2001). "Guided wave interpretation of surface reflection techniques for deep foundation." *Ital. Geotech. J.*, 35(1), 1–37.
- Gassman, S. (1997). "Impulse response evaluation of inaccessible foundations." PhD thesis, Northwestern Univ., Evanston, Ill.
- Hanifah, A. (1999). "Theoretical evaluation of deep foundation using guided wave approach." PhD thesis, Northwestern Univ., Evanston, Ill.
- Pavlakovic, B., Lowe, M., and Cawley, P. (1998). "Guided ultrasonic waves for the inspection of post-tensioned bridges." *Rev. Prog. Quant. Nondestr. Eval.*, 17(B), 1557–1564.
- Popovics, J., Achenbach, J., and Song, W. (1999). "Application of new ultrasound and sound generation methods for testing concrete structures." *Mag. Concrete Res.*, 51(1), 35–44.
- Subramaniam, K., Popovics, J., and Shah, S. (2001). "Determining elastic properties of concrete using vibrational resonance frequencies of standard test cylinders." *Cem., Concr., Aggregate*, in press.
- Thurston, R. (1978). "Elastic waves in rods and clad rods." *J. Acoust. Soc. Am.*, 64(1), 1–37.
- Vaidyanathan, P. (1993). *Multirate systems and filter banks*, Prentice-Hall, Englewood Cliffs, N.J.
- Zemanek, J. (1971). "An experimental and theoretical investigation of elastic wave propagation in a cylinder." *J. Acoust. Soc. Am.*, 51, 265–283.